ELSEVIER

Vibrational Spectroscopy 16 (1998) 95–103

VIBRATIONAL SPECTROSCOPY

In situ analysis of ash deposits from black liquor combustion

Peter Bernath [a,b,*], Scott A. Sinquefield [a,c], Larry L. Baxter [a], Gian Sclippa [a], Celeste M. Rohlfing [a], Michael Barfield [a,d]

[a] *Combustion Research Facility Sandia National Laboratories Livermore, CA 94551-0969, USA*
[b] *Department of Chemistry, University of Waterloo, Waterloo, ON, Canada*
[c] *Department of Chemical Engineering, Oregon State University, Corvalis, OR, USA*
[d] *Department of Chemistry, University of Arizona, Tucson, AZ, USA*

Received 16 May 1997; accepted 17 December 1997

Abstract

Aerosols formed during combustion of black liquor cause a significant fire-side fouling problem in pulp mill recovery boilers. (Black liquor is a recycled by-product formed during the pulping of wood in the paper-making industry). The ash deposits reduce heat transfer effectiveness, plug gas passages, and contribute to corrosion. Both vapors and condensation aerosols lead to the formation of such deposits. The high ash content of the fuel and the low dew point of the condensate salts lead to a high aerosol and vapor concentration in most boilers. In situ measurements of the chemical composition of these deposits is an important step in gaining a fundamental understanding of the deposition process. Infrared emission spectroscopy is used to characterize the composition of thin film deposits resulting from the combustion of black liquor and the deposition of submicron aerosols and vapors. New reference spectra of Na_2SO_4, K_2SO_4, Na_2CO_3 and K_2CO_3 pure component films were recorded and compared with the spectra of the black liquor deposit. All of the black liquor emission bands were identified using our new reference spectra as well as literature data and ab initio calculations. The ab initio calculations predict the locations and intensities of infrared bands for the alkali-containing vapors of interest.

Keywords: Black liquor; Ash deposits; In situ analysis

1. Introduction

Infrared emission spectroscopy of solids is well known, but the technique has not been widely used primarily because bulk and powdered solids tend to give poor spectra due to multiple absorption, emission, and scattering of the radiation before it has a chance to escape the sample [1–3]. However, high quality spectra are obtainable from thin films and small particles with dimensions less than about 100 μm.

Infrared emission spectroscopy is an excellent tool for the characterization of the surface of catalysts and the deposits formed in combustion processes. In general, emission spectroscopy has been an unjustly neglected technique [4]. The use of the technique for characterization of coal and biomass deposits was previously illustrated [5,6]. We illustrate the potential of the technique with the deposits formed during the combustion of black liquor. These

* Corresponding author.

0924-2031/98/$19.00
PII S0924-2031(98)00002-2

deposits turn out to be almost entirely Na_2CO_3 and Na_2SO_4.

Black liquor is a recycled by-product formed during the pulping of wood in the paper-making industry [7]. Na_2S and NaOH are used to break down the complex organic glue, known as 'lignin', that binds wood fibers. In this process large amounts of carbonate are formed from oxidation of the organics, and the sulfide is oxidized to sulfate. After the fibers are removed from the caustic solution, the solution is burned in boilers to recover and reuse the inorganic chemicals and generate process steam and electricity, usually for on-site use. Such boilers are called recovery boilers, with the dominant process and boiler design being that developed by Kraft—hence the term Kraft recovery boilers. As fired, black liquor is approximately one third organics (mostly from the wood), one third inorganics (mostly from the process), and one third water.

The liquor used in this work was diluted to approximately 80% water. In the combustion environment of the recovery boiler, a fraction of the inorganics vaporize and recondense to form submicron aerosols which deposit and foul heat transfer surfaces. The resulting decrease in boiler efficiency motivates the study of these salt film deposits.

The strong bands at 880 cm^{-1} and 1140 cm^{-1} found in the black liquor deposit could be easily assigned to Na_2CO_3 and Na_2SO_4, respectively, but the weaker bands were more difficult to assign. The spectra of Na_2SO_4 and K_2SO_4 solids available in the literature [8–11] were not of sufficient quality, therefore new reference spectra of solid Na_2SO_4, K_2SO_4, Na_2CO_3 and K_2CO_3 were recorded. The comparison of the emission spectra of these salt films with the spectra of the black liquor deposit allowed the identification of all of the unknown bands.

Black liquor combustion generates alkali-containing vapors, predominantly sodium salts (Na_2SO_4 and Na_2CO_3). As gas composition and temperature in a boiler change, a portion of these vapors form condensation aerosols with a mean diameter of about 0.7 μm [12,13]. The aerosols and vapors are carried into the upper furnace, where they accumulate on relatively cool heat transfer surfaces. This paper details in situ detection of the accumulation of these materials on surfaces as a function of time and provides ab initio predictions of the vibrational spectra of the vapors. Some infrared spectra of rare gas matrix-isolated sulfates [14–18] and carbonates [19] are published.

2. Experimental

The Multifuel Combustor (MFC) at the Combustion Research Facility, Sandia National Labs., CA [20] was used to make thin films of the black liquor deposit constituents, Na_2SO_4, K_2SO_4, Na_2CO_3, and K_2CO_3. The MFC is a down-fired, turbulent flow reactor of small pilot-scale size that allows for particle and gas temperature histories to be adjusted over a wide range of conditions. Total fuel residence time can vary from milliseconds to 5 s in the facility. In these experiments, black liquor and pure alkali salts were fired separately in the combustor.

Spectroscopic analyses of thin films collected on simulated boiler tubes in the MFC provided reference spectra and sample spectra, respectively. For the salts, aqueous solutions with concentrations of nominally 100 g/l were aspirated into the top of the combustor and carried through the furnace by a flow of nominally 30 l/s of air. The combustor's gas-fired preheater was not lit, but the silicon carbide (SiC) walls of the combustor were held at a temperature of 1000–1100°C by electrical SiC heating elements.

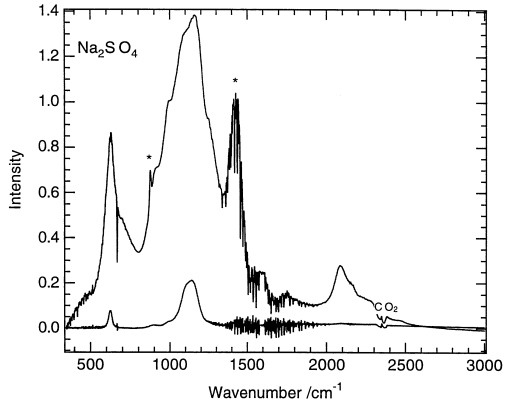

Fig. 1. Sodium sulfate spectrum obtained from combustion tests of pure material in the MFC. Asterisks indicate residual carbonate impurity. The two spectra correspond to different deposit thicknesses. CO_2 bending mode at 667 cm^{-1} can also be seen in absorption. The lower trace is emission from a thin deposit.

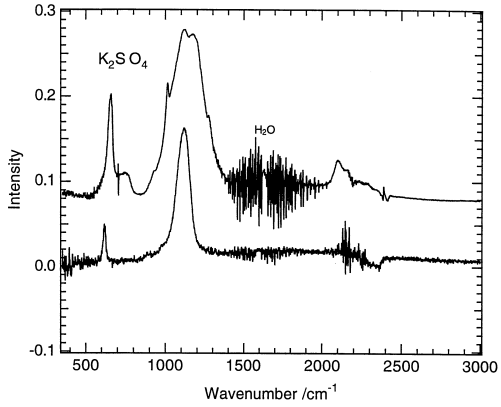

Fig. 2. Potassium sulfate spectrum obtained from combustion tests of pure material in the MFC. The lower trace is emission from a thin deposit.

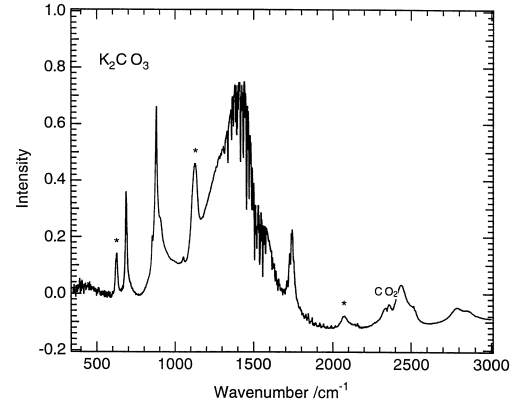

Fig. 4. Potassium carbonate spectrum obtained from combustion tests of pure material in the MFC. Asterisks indicate residual sulfate impurity.

The deposits were collected at the bottom of the combustor on a hollow rotating stainless steel rod 1.7 cm in diameter. The air flow through the combustor maintained the temperature of the rod at about 400°C. The salt deposits on the rod had a thickness of about 100–200 μm at the end of the experiments.

In situ emission spectra of the salt films were recorded at a resolution of 2 cm^{-1} with a Biorad Model FTS 40/60 Fourier transform infrared spectrometer (FT-IR) equipped with a KBr-supported beamsplitter and a DTGS detector. Spectra of the original rod surface were recorded prior to salt accumulation and subtracted from the salt spectra. Scans were collected over 10 min (256 scans) and were co-added for each of the original surface and the salt spectra. The resulting spectra (Figs. 1–4) exhibited high signal-to-noise ratios and good peak definition in the mid-infrared (350–3000 cm^{-1}) region. More information about infrared emission spectroscopy is available in a recent review [4].

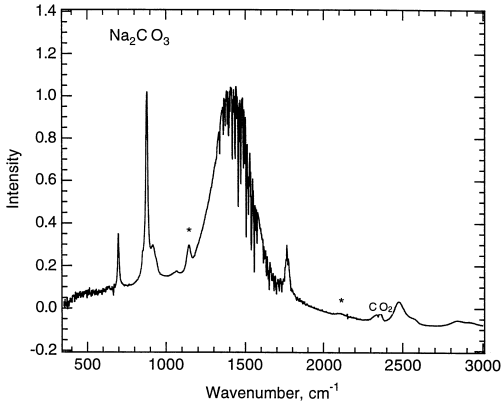

Fig. 3. Sodium carbonate spectrum obtained from combustion tests of pure material in the MFC.

The deposit from the black liquor was prepared in a similar manner as the reference salt films. In this case the temperature of the walls of the furnace was about 900°C while the rotating stainless steel rod was at 300°C. The black liquor contained about 10% organic material, mainly lignin and its degradation products, that burned before the residual deposit formed. A time series of emission spectra (Fig. 5) of the deposit on the rod was recorded with the spectrometer. For each spectrum, 16 scans were co-added in 0.5 min of integration. After 52 min the black liquor flow was stopped and a final spectrum (Fig. 6) was measured.

3. Results and discussion

The deposit from the black liquor has an infrared spectrum (Fig. 6) with numerous vibrational bands. The major bands and their assignments, compared with the reference spectra, are listed in Table 1. The sharp, strong band at 880 cm^{-1} is the characteristic out of plane bending mode $\nu_2(a''_2)$ of the CO_3^{2-} ion [21–25]. The CO_3^{2-} ion has D_{3h} symmetry with modes $\nu_4(e')$ 681 cm^{-1}, $\nu_2(a''_2)$ 880 cm^{-1}, $\nu_1(a'_1)$ 1067 cm^{-1} and $\nu_3(e')$ 1380 and 1440 cm^{-1} in dilute

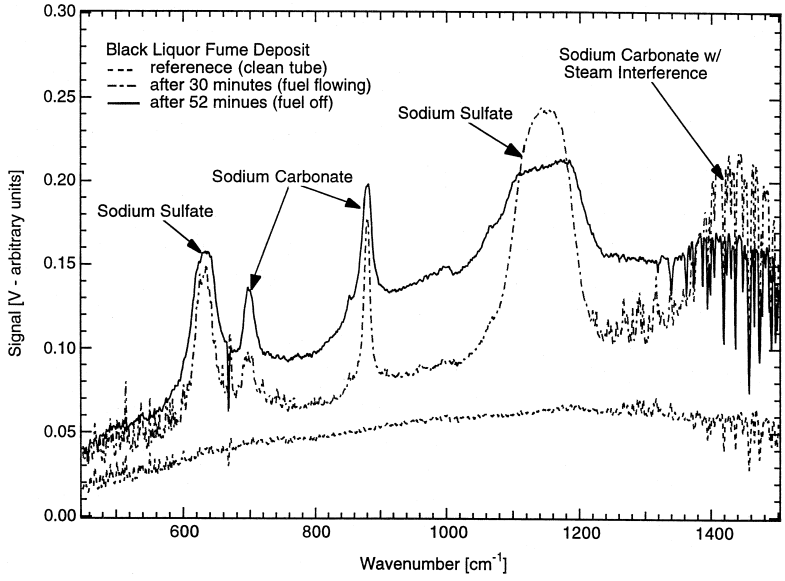

Fig. 5. A time series of black liquor deposit spectra with peaks assignments. The CO_2 bending mode at 667 cm^{-1} can also be seen.

solution. The doubly degenerate $\nu_3(e')$ mode experiences reduced symmetry in solution and appears as two bands [21]. Only the a_2'' and e' modes are infrared active for the D_{3h} point group but in condensed phases the effective symmetry is lower and other modes can appear [21].

The strong band (Fig. 6) at 1148 cm^{-1} in the black liquor deposit is characteristic of the antisymmetric stretch vibration of the tetrahedral SO_4^{2-} ion. In dilute solution, the SO_4^{2-} ion (T_d point group) has modes $\nu_2(e)$ 450 cm^{-1}, $\nu_4(t_2)$ 611 cm^{-1}, $\nu_1(a_1)$ 983 cm^{-1} and $\nu_3(t_2)$ 1105 cm^{-1} [25,26]. Only the t_2 modes are infrared active but the other modes can appear in condensed phases [27,28].

In condensed phases, it is common to observe a shift in the functional group frequencies. In addition, agreement between literature reference spectra and observed feature locations is complicated by several factors. Literature references are predominately derived from pure, room-temperature samples of micronized mineral pressed in a KBr wafer and exam-

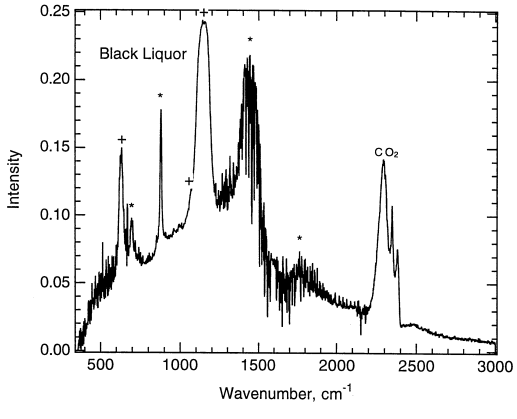

Fig. 6. Black liquor deposit spectra near the end of the combustion test, illustrating fully developed peaks of sulfate (+) and carbonate (∗).

Table 1
Vibrational band positions of the black liquor deposit (cm^{-1})

Position	Assignment[a]
631	Na_2SO_4, 624
698	Na_2CO_3, 699
853	Na_2CO_3, 854
880	Na_2CO_3, 880
1000	Na_2SO_4, 995
1066	Na_2CO_3, 1069
1148	Na_2SO_4, 1137
~1400	Na_2CO_3, ~1400
1765	Na_2CO_3, 1767
2117	Na_2SO_4, 2087
2470	Na_2CO_3, 2476

[a] This work.

ined in transmission using an FTIR or other suitable spectroscopic instrument. By contrast, these in situ emission spectra of the ash deposits containing many inorganic phases are collected at combustion temperatures on deposition probes. The sample mixture, morphology, and temperature may alter the spectral signatures. Mixtures of samples may cause weak or broad features to become indistinguishable from either the background or features from other species. Temperature changes in a material can change the location of a room temperature feature by a few wavenumbers (usually less than 10 cm^{-1}) at 400°C [29] and as much as 40 cm^{-1} at 1700°C for halide and oxide crystal [30]. The changes can either increase or decrease the wavenumber of a band, although decreases in wavenumber are most common. Changes are also more pronounced for crystalline material than for amorphous material [31] and are more significant at low wavenumbers than at high wavenumbers. Deposit thickness variations for pure, thin films have been reported for materials of interest to ash deposition [32] and in the literature for liquids [33]. Deposit thickness can also have a pronounced effect on feature shapes and apparent position. The combination of ab initio calculation and literature reference spectra combined provide definitive assignment of the observed features of our spectra.

While the 880 cm^{-1} CO_3^{2-} and 1048 cm^{-1} SO_4^{2-} peaks are readily assigned, the interpretation of the smaller peaks is much less certain. In addition the cations associated with the SO_4^{2-} and CO_3^{2-} anions are not certain. The elemental composition of the black liquor was found to be C (34.8%), H (3.0%), O (35.0%), Na (22.6%), K (0.62%), S (2.9%), Cl (0.67%) and N (0.08%) on a dry basis. The remainder consists of inert material such as Fe_2O_3 and SiO_2 (i.e., dirt, sand, etc.) that enters the process with the wood. The potassium also enters the process as a constituent of the wood. Thus the deposit could contain K_2SO_4 and K_2CO_3 as well as Na_2SO_4 and Na_2CO_3. Reference spectra of pure Na_2SO_4 (Fig. 1), K_2SO_4 (Fig. 2), Na_2CO_3 (Fig. 3), and K_2CO_3 (Fig. 4) were therefore recorded for comparison purposes and the bands measured (Tables 1, 2 and 5).

The observed sulfate bands were readily assigned (Table 5) on the basis of previous work [25–28]. The forbidden $\nu_2(e)$ mode near 450 cm^{-1} was too weak to identify but the symmetric stretching vibration

Table 2
Observed carbonate band positions (cm^{-1})

Mode	CO_3^{2-} solution[a]	Na_2CO_3 film	K_2CO_3 film
$\nu_4(e')$	681	699	686
		854[b]	852[b]
$\nu_2(a_2'')$	880	880	879
		917[b]	903[b]
$\nu_1(a_1')$	1067	1069	1053
$\nu_3(e')$	1380;1412	~1400	~1400
$2\nu_2$	–	1767	1738
$\nu_1+\nu_3$	–	2476	2437
$\nu_1+\nu_3$	–	2562[b]	2516[b]
$2\nu_3$	–	2843	2788
$2\nu_3$	–	2911[b]	2852[b]

[a]Ref. [21].
[b]Shoulder.

$\nu_1(a_1)$ appeared as a shoulder. Two weak bands appeared near 2100 cm^{-1} and are assigned in the literature [27] as the $\nu_1+\nu_3$ combination band and the $2\nu_3$ overtone. The $\nu_1+\nu_3$ assignment is plausible since the predicted band position is 2132 cm^{-1}, but the $2\nu_3$ assignment for the 2153 cm^{-1} band (Na_2SO_4) is less certain since $2\times\nu_3 = 2274$ cm^{-1}.

The assignments for the Na_2CO_3 and K_2CO_3 spectra were also straightforward (Table 2). All of the four CO_3^{2-} modes were found as well as several overtones and combination bands. Interestingly the overtones and combination bands which contain ν_3 are all split into two bands. This splitting of the ν_3 fundamental is well-known in solutions and melts [21] but is not obvious (Figs. 3 and 4) in the spectra of the solids. The ν_3 fundamental is badly overlapped up by water vapor in our spectra.

The direct comparison of Figs. 1–4 with Fig. 6 allows all of the bands in the black liquor deposit to

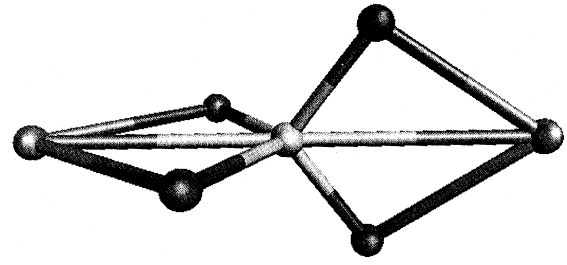

Fig. 7. Structure of the sodium sulfate molecule. The slightly distorted sulfate tetrahedron is in the middle and the two sodium atoms are on opposite edges.

Table 3
Fundamental vibrational modes of Na_2SO_4 calculated ab initio at MP2/6-31G* level

Mode	Frequency (cm^{-1})	Comment
$\nu_{11}(e)$	68(54)[a]	NaO_2 bend
$\nu_{10}(e)$	272(4)	NaO_2 bend
$\nu_3(a_1)$	276(0)	NaO_2 symmetric stretch
$\nu_7(b_2)$	359(140)	NaO_2 antisymmetric stretch
$\nu_4(b_1)$	379(0)	$\nu_2(e)$ 450 cm^{-1} SO_4^{-2} bend
$\nu_2(a_1)$	525(0)	$\nu_2(e)$ 450 cm^{-1} SO_4^{-2} bend
$\nu_9(e)$	584(36)	$\nu_4(t_2)$ 611 cm^{-1} SO_4^{-2} bend
$\nu_6(b_2)$	642(42)	$\nu_4(t_2)$ 611 cm^{-1} SO_4^{-2} bend
$\nu_1(a_1)$	938(0)	$\nu_1(a_1)$ 983 cm^{-1} SO_4^{-2} symmetric stretch
$\nu_8(e)$	1104(383)	$\nu_3(t_2)$ 1105 cm^{-1} SO_4^{-2} antisymmetric stretch
$\nu_5(b_2)$	1146(668)	$\nu_3(t_2)$ 1105 cm^{-1} SO_4^{-2} antisymmetric stretch

[a]Calculated band strengths in km/mol are in parentheses.

be assigned (Table 1). There is no clear evidence for K_2SO_4 and K_2CO_3 in the deposit, but they cannot be ruled out because most of their band positions are nearly coincident with the corresponding Na_2SO_4 and Na_2CO_3 bands. They would, in any case, be a fairly minor constituent of the deposit based on the black liquor composition.

Surprisingly the high temperature behavior of Na_2SO_4 and Na_2CO_3 is not well established. The decomposition reactions:

$$Na_2SO_4(l) \leftrightarrow 2Na(g) + SO_2(g) + O_2(g)$$

$$Na_2CO_3(l) \leftrightarrow Na_2O(s) + CO_2(g)$$

certainly occur, but a substantial fraction of the high temperature vapors are Na_2SO_4 [34,35] and Na_2CO_3 [36] molecules. The extent of decomposition is typically measured by mass spectrometry. Since the parent ions of molecules such as Na_2SO_4 and Na_2CO_3 tend to fragment, mass spectrometry often underestimates the concentration of inorganic species. Molten Na_2SO_4 and Na_2CO_3 are also very corrosive, so the container material may influence the decomposition. Thus, the extent of decomposition is not reliably known for Na_2SO_4 and Na_2CO_3 at high temperatures.

The existence of molecular Na_2SO_4 and K_2SO_4 in the gas phase is supported by the infrared and Raman spectra recorded for isolated molecules trapped in inert matrices at low temperatures [16,17]. Infrared absorption spectra of K_2CO_3 (but not Na_2CO_3) have also been published [19].

These results all suggest that molecular Na_2SO_4 and Na_2CO_3 will be important species in the fume produced in Kraft black liquor recovery boilers. As a prelude to the gas phase study of these molecules, we completed ab initio quantum chemical calculations of the infrared spectra. The Gaussian 92 program [37] was used to approximately solve the electronic Schrödinger equation with the standard 6-

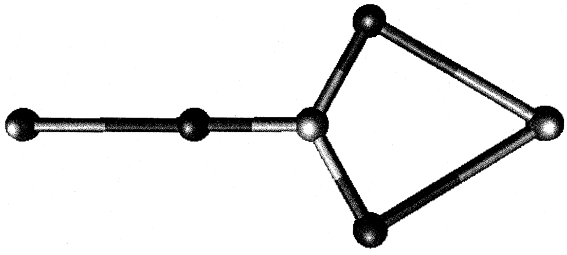

Fig. 8. One of two alternate structures of the sodium carbonate molecule (compare Fig. 9). This structure is planar with the carbonate group in the center and has a higher energy than that of Fig. 9.

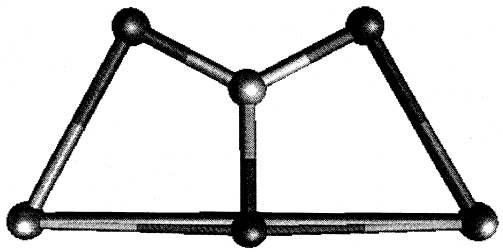

Fig. 9. One of two alternate structures of the sodium carbonate molecule (compare Fig. 8). There are two equivalent bidentate sodium atoms around the central carbonate group.

Table 4
Fundamental vibrational modes of Na_2CO_3 calculated ab initio at MP2/6-31G* level

Mode	Frequency[a], cm^{-1}	Comment
$\nu_8(b_1)$	96(52)	
$\nu_6(a_2)$	107(0)	
$\nu_5(a_1)$	206(22)	
$\nu_4(a_1)$	357(48)	$Na–O_2$ vibrations
$\nu_{12}(b_2)$	370(21)	
$\nu_{11}(b_2)$	384(112)	
$\nu_3(a_1)$	699(1)	$\nu_4(e')$ 681 cm^{-1} CO_3^{-2} in plane bend
$\nu_{10}(b_2)$	738(12)	$\nu_4(e')$ 681 cm^{-1} CO_3^{-2} in plane bend
$\nu_7(b_1)$	842(22)	$\nu_2(a_2'')$ 880 cm^{-1} CO_3^{-2} out of plane bend
$\nu_2(a_1)$	994(100)	$\nu_1(a_1)$ 1067 cm^{-1} CO_3^{-2} symmetric stretch
$\nu_1(a_1)$	1347(565)	$\nu_3(e')$ 1440; 1380 cm^{-1} CO_3^{-2} antisymmetric stretch
$\nu_9(b_2)$	1620(748)	$\nu_3(e')$ 1440; 1380 cm^{-1} CO_3^{-2} antisymmetric stretch

[a]Calculated intensities in km/mol are in parentheses.

31G* basis set and electron correlation at the MP2 level. Geometries were optimized at the MP2/6-31G* level of theory and the vibrational frequencies and intensities were calculated.

For the Na_2SO_4 molecule the lowest energy structure has D_{2d} symmetry (Fig. 7). This structure is consistent with the matrix-isolation spectra [16] as well as the electron diffraction [38] and molecular beam deflection data [39] on the isovalent Cs_2SO_4 molecule. The calculated optimized geometry has a S–O bond length of 1.517 Å and a Na–O bond length of 2.205 Å. S–O bond lengths are typically 1.47 Å for the SO_4^{2-} anion in crystals [14], 1.471 Å derived from the electron diffraction results on Cs_2SO_4 [39], and 1.48 Å calculated for Li_2SO_4 [14]. The O–S–O bond angles are calculated to be 107.3° facing a Na atom and 110.6° facing away from Na.

The predicted vibrational frequencies and intensities of Na_2SO_4 are reported in Table 3. The only experimental values available for comparison are the N_2 matrix values [16] of 1131 cm^{-1} $\nu_5(b_2)$, 1103 and 1097 cm^{-1} $\nu_8(e)$, 961 cm^{-1} $\nu_1(a_1)$, 640 cm^{-1} $\nu_6(b_2)$ and 610 cm^{-1} $\nu_9(e)$.

Similar ab initio calculations for Na_2CO_3 were carried out for two molecular geometries of C_{2v} symmetry (Figs. 8 and 9, Table 4). The matrix

Table 5
Observed sulfate band positions (in cm^{-1})

Mode	SO_4^{-2} solution[a]	Na_2SO_4 film[b]	Na_2SO_4 solid[a]	Na_2SO_4 melt[c]	K_2SO_4 film[b]	K_2SO_4 solid[a]	K_2SO_4 melt[c]
$\nu_2(e)$	451	–	–	440	–	–	–
			612			612	
$\nu_4(t_2)$	613	624	638	Saturated	619	619	Saturated
			643[d]		711[d]	654[d]	
$\nu_1(a_1)$	981	995[d]	988	–	975	983	–
			1105				
$\nu_3(t_2)$	1104	1137	1124	Saturated	1120	1101	Saturated
			1175[d]				
$\nu_1 + \nu_3(t_2)$	–	2087	–	2060	2064	–	2020
$2\nu_3(t_2)$?	–	2153[d]	–	2190[d]	2113[d]	–	2150[d]

[a]Ref. [26].
[b]This work.
[c]Ref. [27].
[d]Shoulder.

isolation results are unable to distinguish between the two possibilities but calculations on Li_2CO_3 [40] indicate that the structure with two bidentate bonds to the Na atoms (Fig. 9) as the ground state. For Na_2CO_3 our calculations predict that the structure in Fig. 8 is a local minimum in the total energy, but it lies 20.4 kcal/mol above the structure in Fig. 9. The lowest energy structure (Fig. 9) has two calculated C–O bond lengths of 1.285 Å (on the top) and one of 1.367 Å (pointing down). The Na–O bond lengths are 2.170 Å (on top) and 2.185 Å (on bottom). The calculated O–C–O angles are close to 120° with two values of 118.1° facing Na atoms and 123.9° facing away from Na atoms. The calculated vibrational frequencies and intensities are reported in Table 4. There are no suitable experimental Na_2CO_3 values for comparison.

4. Conclusions

Inorganic material accumulating on surfaces during black liquor combustion lends itself to analysis by emission FTIR spectroscopy. Properly instrumented laboratory reactors and diagnostics allow the determination of emission spectra from thin films (100 μm) of alkali salts and of black liquor ash deposits on simulated heat transfer surfaces. Spectral analysis indicates agreement between the assignment of bands, using ab initio calculations in all cases and literature values in some cases. Spectra with good signal-to-noise ratios and well-defined structure are obtainable from both pure materials and mixed materials generated by the combustion of industrial feedstreams.

Ab initio calculations also predict the band locations and intensities of alkali salt vapors, whose existence in practical combustion systems is suspected but has yet to be confirmed. The formation of ash deposits in the upper furnace of recovery boilers is dependent primarily on the concentrations and properties of these salt vapors, their condensation aerosols, and their reaction products. These data and calculations provide baseline information for quantitatively determining vapor concentrations and demonstrate the determination of the resulting ash deposits from such combustion systems.

References

[1] P.V. Huong, Advances in Infrared and Raman Spectroscopy, in: R.J.H. Clark, R.E. Hester (Eds.), Heyden, London, 1978.
[2] G. Fabbri, P. Baraldi, Appl. Spectrosc. 26 (1972) 593–599.
[3] P. Baraldi, G. Fabbri, Spectrochim. Acta 39A (1983) 669–675.
[4] P.F. Bernath, Chem. Soc. Rev. 25 (1996) 111–115.
[5] L.L. Baxter, Engineering Foundation Conference on The Impact of Ash Deposition on Coal-Fired Plants, 1993.
[6] L.L. Baxter, G.H. Richards, D.K. Ottesen, J.N. Harb, Energy Fuels 7 (1993) 755–760.
[7] T.N. Adams, W.J. Fredrick, Kraft Recovery Boiler Physical and Chemical Processes, American Paper Institute, 1988.
[8] The Infrared Spectra Handbook of Inorganic Compounds, Sadtler Research Laboratories, a Division of Bio-Rad Laboratories, Philadelphia, 1984.
[9] R.A. Nyquist, R.O. Kagel, Infrared Spectra of Inorganic Compounds, Academic Press, San Diego, 1971.
[10] J.R. Ferraro (Eds.), The Sadtler Infrared Spectra Handbook of Minerals and Clays, Sadtler Research Laboratories, a Division of Bio-Rad Laboratories, Philadelphia, 1982.
[11] A.M. Vassallo, K.S. Finnie, Appl. Spectrosc. 46 (1992) 1477–1482.
[12] P. Mikkanen, E.I. Kauppinen, E.I. Jokiniemi, S.A. Sinquefield, W.J. Frederick, M. Mäkinen, AIChE Symp. Ser. 90 (1994) 46–54.
[13] P. Mikkanen, E.I. Kauppinen, J.K. Jokiniemi, S.A. Sinquefield, W.J. Frederick, TAPPI 77 (1994) 81–84.
[14] F. Ramondo, L. Bencivenni, R. Caminiti, C. Sadun, Chem. Phys. 151 (1991) 179–186.
[15] M. Spoliti, L. Bencivenni, S.N. Cesaro, R. Geghil, M. Maltese, J. Mol. Struct. 74 (1981) 297–299.
[16] R.M. Atkins, K.A. Gingerich, Chem. Phys. Lett. 53 (1978) 347–349.
[17] A.A. Belyaeva, M.I. Dvorkin, L.D. Shcherba, J. Struct. Chem. 21 (1980) 738–744.
[18] H.M. Nagarathna, L. Bencivenni, K.A. Gingerich, J. Chem. Phys. 81 (1984) 591–598.
[19] J.S. Ogden, S.J. Williams, J. Chem. Soc., Dalton Trans., 1981, pp. 456–462.
[20] L.L. Baxter, Combust. Flame 90 (1992) 174–184.
[21] J.B. Bates, M.H. Brooker, A.S. Quist, G.E. Boyd, J. Phys. Chem. 76 (1972) 1565–1571.
[22] J.B. Bates, G.E. Boyd, Appl. Spectrosc. 27 (1973) 1973.
[23] J.B. Bates, in: J.R. Ferraro, L.J. Basile (Eds.), Fourier Transform Infrared Spectroscopy, Academic Press, New York, 1978.
[24] M.H. Brooker, J.B. Bates, J. Chem. Phys. 54 (1971) 4788–4796.
[25] K. Nakamoto, Infrared and Raman Spectroscopy of Inorganic and Coordination Compounds, Wiley, New York, 1986.
[26] S.D. Ross, Spectrochim. Acta 18 (1962) 1575–1578.
[27] R.E. Hester, K. Krishnan, J. Chem. Phys. 43 (1965) 479–482.
[28] G.E. Walrafen, D.E. Irish, T.F. Young, J. Chem. Phys. 37 (1962) 662–670.

[29] C.F. Bohren, D.R. Huffman, Absorption and Scattering of Light by Small Particles, Wiley, New York, 1983.
[30] J.R. Jasperse, A. Kahan, J.N. Plendl, Phys. Rev. 146 (1966) 526–542.
[31] S.S. Mitra, S. Nudelman (Eds.), Far-Infrared Properties of Solids, Plenum, New York, 1970.
[32] L.L. Baxter, D.R. Hardesty, Sandia National Laboratories, The Fate of Mineral Matter During Pulverized Coal Combustion: Quarterly Report for July–September 1992, Sandia Report, SAND93-8230 (1993).
[33] J. Hvistendahl, E. Rytter, H.A. Øye, Appl. Spectrosc. 37 (1983) 182–187.
[34] D. Cubicciotti, F.J. Keneshea, High Temp. Sci. 4 (1972) 32–40.
[35] D.R. Lide (Eds.), Handbook of Chemistry and Physics, CRC Press, Boca Raton, FL, 1995.
[36] L.L. Simmons, L.F. Lowdeon, T.C. Ehlert, J. Chem. Phys. 81, 706–709.
[37] Gaussian 92, Revision C, M.J. Frisch, G.W. Trucks, M. Head-Gordon, P.M.W. Gill, M.W. Wong, J.B. Foresman, B.G. Johnson, H.B. Schlegel, M.A. Robb, E.S. Replogle, R. Gompets, J.L. Andres, K. Raghavachari, J.S. Binkley, C. Gonzalez, R.L. Martin, D.J. Fox, D.J. Defrees, J. Baker, J.J.P. Stewart, J.A. Pople, Gaussian, Pittsburgh, PA, 1992.
[38] V.A. Kulikov, V.V. Ugarov, N.G. Rambidi, J. Struct. Chem. 23 (1982) 158–160.
[39] A. Buchler, J.L. Stauffer, W. Klemperer, J. Chem. Phys. 46 (1967) 605–608.
[40] F. Ramondo, L. Bencivenni, J. Mol. Struct. 221 (1990) 169–174.